Multiscale approach of mechanical behaviour of SiC/SiC composites : elastic behaviour at the scale of the tow

Camille Chateau, Lionel Gélébart, Michel Bornert, Jérôme Crépin, Daniel Caldemaison

TECHNISCHE MECHANIK, 30, 1-3, (2010), 45 – 55
submitted: October 30, 2009

Multiscale approach of mechanical behaviour of SiC/SiC composites: elastic behaviour at the scale of the tow

C. Chateau, L. Gélébart, M. Bornert, J. Crépin, D. Caldemaison

SiC/SiC composites are candidates for structural applications at elevated temperatures in the context of the development of the 4th generation of nuclear reactors. A multiscale approach is under development to construct a predictive modelling of their complex mechanical behaviour due to their heterogeneous microstructure. This approach is based on two scale transitions: from the fibres/matrix microstructure to the tow and from the tow to the woven composite, each scale presenting a significant residual porosity. This paper focuses on the first scale transition and on the modelling of the elastic behaviour of the tow at room temperature. A microstructural investigation of several tows in a 2D SiC/SiC specimen has been conducted using scanning electron microscopy to get statistical data on microstructural characteristics by image analysis in order to generate a virtual microstructure. The elastic problem of homogenisation is numerically solved by means of finite element techniques. The simulations performed on various volumes show noticeable fluctuations of the apparent behaviour: so separation of length scales is not satisfied in this material. Nevertheless, this problem is neglected in a first approximation and the homogeneous equivalent behaviour is evaluated by averaging the apparent behaviours of several volume elements – smaller than the Representative Volume Element (RVE) – called Statistical Volume Elements (SVEs). Finally, influence of porosity and pores' morphology is quantified.

1 Introduction

In the context of the development of the 4th generation of nuclear reactors, SiC/SiC composites are candidates for structural applications at elevated temperatures. The composites under investigation are elaborated from a fibrous preform on the base of tows constituted by 500 SiC fibres. A Chemical Vapor Infiltration process (CVI) is used to deposit a thin interphase of pyrocarbon and to densify the composites with SiC matrix. Because of the CVI process, the materials cannot be fully densified and a residual porosity appears within the composites. The composites, as the porosity, may be described at two different scales: the scale of the tow (micro-porosity, between the fibres) and the scale of the woven composite (macro-porosity, between the tows). A multiscale approach is under development to build a predictive model of their complex mechanical behaviour taking into account their heterogeneous microstructure (Gélébart and Colin (2009); Gélébart et al. (in press)). Indeed such a model is necessary to predict the effects of the microstructural variability – especially due to the CVI process and the components arrangement – on the macroscopic mechanical behaviour.

This paper focuses on the first scale transition and on the modelling of the elastic behaviour of the tow at room temperature. A microstructural characterisation of a 2D SiC/SiC specimen is conducted using scanning electron microscopy (SEM). A sufficient number of tows are observed to get statistical data on microstructural characteristics by image analysis (porosity, fibres diameter . . .). Then these data are used in a numerical procedure to generate a virtual microstructure. At last, finite element techniques are used to numerically solve the elastic problem of homogenisation. The simulations performed on various volumes show fluctuations of the apparent behaviour which point out separability of scales issues. Nevertheless, this problem is neglected in a first approximation and the homogeneous equivalent behaviour is evaluated. Finally, the effects of the pores' morphology and the volume fraction of porosity are discussed, showing the impact of the quality of the CVI process on the mechanical behaviour.

2 Homogenisation process

2.1 Generation of virtual microstructure

2.1.1 Characterisation of the microstructure

The investigated material is a 2D woven SiC/SiC composite elaborated from a fibrous preform on the base of tows constituted by 3rd generation SiC fibres (Hi-Nicalon S). A thin interphase of PyC and the SiC matrix are deposited using a Chemical Vapor Infiltration process (CVI). The material can not be fully densified because of the CVI process and a residual porosity appears within the composite (Figure 1a), especially within the tow (micro-porosity). Figure 1b shows the microstructure of the composite and illustrates the heterogeneous distribution of fibres and porosity. Six tows, like the one presented on Figure 2, were randomly chosen in a composite sample section to statistically characterize the microstructure using SEM. Stitched images built from several high resolution images – the image on Figure 2 needed five 4096x3773 pixels images (1 pixel ≈ 0.07 µm) – are used to get statistical data about the microstructure using image analysis. The process returns images containing only the fibres or only the porosity (see Figure 2) and permits to determine both position as well as diameter of each fibre and both position and area of each pore within the tow.

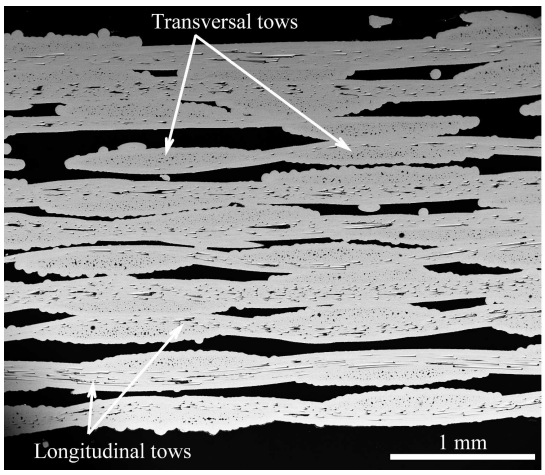

(a) Transversal section of the 2D composite

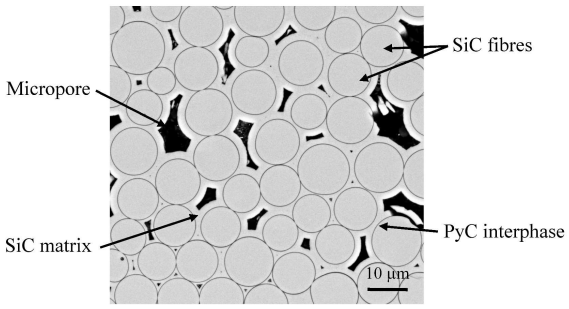

(b) Zoom into a transversal tow

Figure 1: SEM-FEG observations of the composite (backscattered electrons)

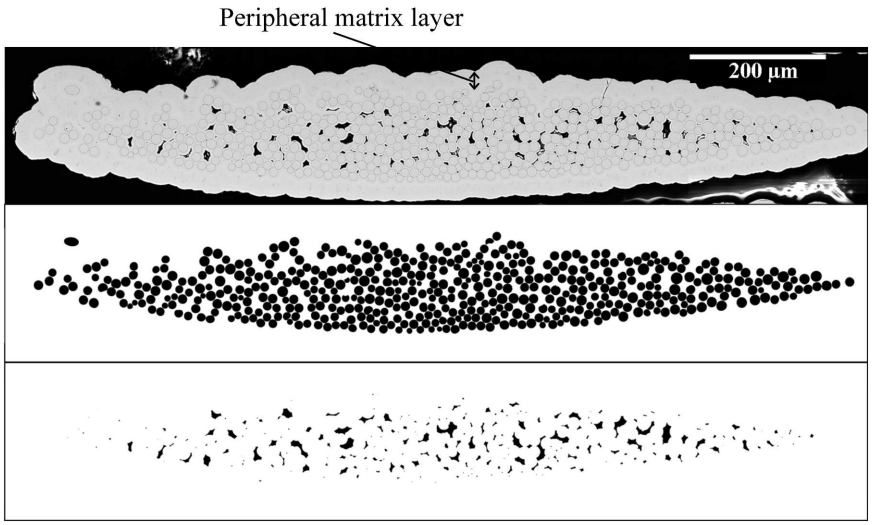

Figure 2: A tow (transverval section) and results of image analysis containing only the fibres or only the pores

The microstructural investigation reveals that a tow contains approximately 500 fibres randomly distributed in the plane perpendicular to the fibres direction. As shown on Figure 3, the fibres diameter is not constant and has an average value of $13\ \mu\mathrm{m}$. Moreover fibres are often stuck to their neighbours. Surface fractions of fibres range from 53% to 64%, and surface fractions of porosity from 3% to 5%, depending on the considered tow. These surface fractions are evaluated considering the internal area without taking into account the peripheral thick matrix layer (see Figure 2). Finally the thickness of the matrix deposit is qualitatively estimated at $3\ \mu\mathrm{m}$ on average, but it can fluctuate within some tows approximately between $1\ \mu\mathrm{m}$ and $5\ \mu\mathrm{m}$. The main characteristics of the microstructure are summarized in Table 1.

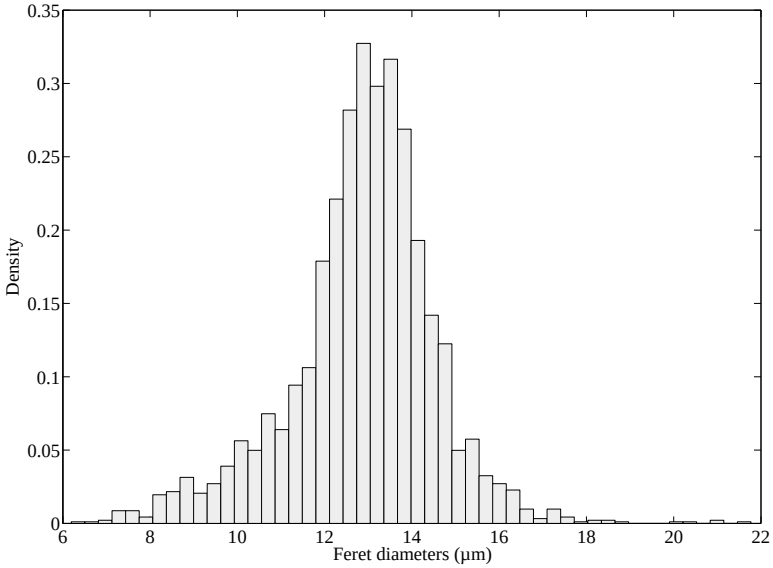

Figure 3: Normalized histogram of fibres diameters in the 6 tows

Distribution of fibres diameters	
Average	$13\ \mu\mathrm{m}$
Standard deviation	$1.7\ \mu\mathrm{m}$
Mean surface fraction	
Fibres	58%
Porosity	4.1%
Minimum distance between fibres	$0\ \mu\mathrm{m}$
Matrix thickness	$\approx 3\ \mu\mathrm{m}$

Table 1: Main microstructural characteristics

2.1.2 Microstructure generation

Results of the microstructural characterisation are then used to generate a virtual microstructure representative of the observations. The microstructure is supposed to be invariant in the direction of the fibres, so random 2D cross-sections are generated. Fibres – the diameters of which follow a normal distribution with parameters cited in Table 1 – are randomly placed one by one on a far larger area than the tow (at least 5000 fibres) in order to obtain the desired surface fraction of fibres. Each fibre position is randomly drawn from a uniform distribution. The position is not accepted as long as it overlaps with fibres already placed. To avoid trouble during the meshing of the geometry, the minimum distance between fibres is taken to a small value ($0.05\ \mu\mathrm{m}$). However, it is very difficult and time consuming to generate high surface fraction with this sequential generation. Consequently a composite with a fibre surface fraction of 55% – on average in the large area – instead of the 58% measured is analyzed. The matrix thickness – assumed to be constant within the tow – is defined to fit the right surface fraction of porosity. The identified thickness value, $3.6\ \mu\mathrm{m}$, matches with the experimental observations (see Table 1).

A high number of Volume Elements (VEs, Figure 4) of different sizes have been generated in this manner by extracting the area of interest inside the large virtual microstructure. Procedures to build the geometry and the 2D

mesh are developed using the Salome platform (http://www.salome-platform.org). The 3D mesh is generated as an extrusion of the 2D mesh.

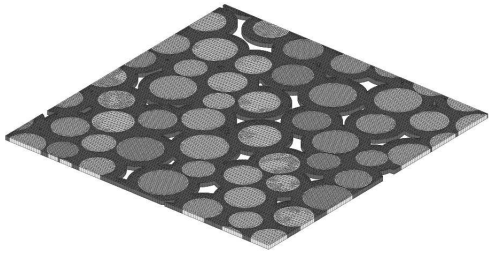

Figure 4: Example of a meshed VE

2.1.3 Materials properties

Fibres and matrix are supposed to be linearly elastic and isotropic with a Young's modulus equal to 372 and 400 GPa, respectively, and an identical Poisson's coefficient equal to 0.18. In fact, even if there is probably a crystallographic texture due to the SiC growth during the CVI process, the resulting anisotropy is negligible in comparison with the effect of the porosity.

2.2 Mechanical calculations and boundary conditions (calculation of apparent behaviour)

The apparent stiffness tensor ($\mathbf{K}^{app}$) of a VE is the 4$^{\text{th}}$ order tensor which links the averages of strain and stress tensors on the volume Ω of the VE (see equations (1) and (2)). When the VE is large enough (the Representative Volume Element, RVE), the apparent behaviour does no longer depend on the considered statistical realisation nor on the boundary conditions. This limit determines the homogeneous equivalent behaviour (or effective behaviour $\mathbf{K}^{eff}$). But the homogeneous equivalent behaviour can be used at the larger scale only if the RVE is far smaller than the structure. Indeed the RVE has to be large enough to be representative but small enough compared to the structure to use the homogeneous equivalent behaviour at the larger scale. This defines the separability of the scales criterion.

$$\langle \epsilon \rangle = \frac{1}{V_\Omega} \int_\Omega \epsilon \, dV, \; \langle \sigma \rangle = \frac{1}{V_\Omega} \int_\Omega \sigma \, dV \tag{1}$$

$$\langle \sigma \rangle = \mathbf{K}_1^{app} : \langle \epsilon \rangle \text{ , for all load cases} \tag{2}$$

The apparent behaviour can also be defined as the 4$^{\text{th}}$ order tensor linking the volume average strain tensor to the volume average of the energy density (see equation (3)). This definition ensures the symmetry of $\mathbf{K}_2^{app}$, while it might not be the case with the first definition of $\mathbf{K}_1^{app}$.

$$\frac{1}{2} \; \langle \epsilon : \mathbf{K} : \epsilon \rangle = \frac{1}{2} \; \langle \epsilon \rangle : \mathbf{K}_2^{app} : \langle \epsilon \rangle \text{ , for all load cases} \tag{3}$$

The Hill condition (see equation (4)) – which is the expression of the equality between the macroscopic work and the spatial average of the microscopic work – ensures the equivalence of the two definitions of $\mathbf{K}^{app}$, when it is satisfied by the local fields σ and ϵ (Bornert et al. (2001)), for all load cases.

$$\langle \sigma \rangle : \langle \epsilon \rangle = \langle \sigma : \epsilon \rangle \tag{4}$$

It is possible to calculate one by one the 36 coefficients of the tensor with 6 independent load cases coupling the results together. Solving the system (5) – where I refers to a particular load case – leads to identify coefficients of $\mathbf{K}_1^{app}$ and system (6) with the coefficients of $\mathbf{K}_2^{app}$.

$$\langle\sigma\rangle^I = \mathbf{K}_1^{app} : \langle\epsilon\rangle^I \,,\ \forall I \in [1,6] \tag{5}$$

$$\langle\sigma^I : \epsilon^J\rangle = \frac{1}{2}\,\bar{\epsilon}^I : \mathbf{K}_2^{app} : \bar{\epsilon}^J,\ \forall (I,J) \in [1,6]^2 \tag{6}$$

The boundary conditions on the VE preferably have to satisfy the Hill condition, which leads to three types of boundary conditions defined on the boundary $\partial\Omega$ of the volume Ω (Hazanov and Amieur (1995); Jiang et al. (2002)): the kinetic uniform boundary conditions (KUBC, equation (7)), the static uniform boundary conditions (SUBC, equation (8)) and the mixed uniform boundary conditions (MUBC, equation (9)). Note that the MUBC, unlike SUBC and KUBC, do not define a specific set of boundary conditions but refer to a wide family of boundary conditions. Periodic boundary conditions (PBC) are also often used and satisfy the Hill condition (equation (10)). In the following, **t**, **u** and **L** refer to the traction, displacement and periodicity vectors, respectively.

$$\mathbf{u}(\mathbf{x}) = \langle\epsilon\rangle \cdot \mathbf{x},\ \forall \mathbf{x} \in \partial\Omega \tag{7}$$

$$\mathbf{t}(\mathbf{x}) = \langle\sigma\rangle \cdot \mathbf{n},\ \forall \mathbf{x} \in \partial\Omega \tag{8}$$

$$(\mathbf{t}(\mathbf{x}) - \langle\sigma\rangle \cdot \mathbf{n}) \cdot (\mathbf{u}(\mathbf{x}) - \langle\epsilon\rangle \cdot \mathbf{x}) = 0,\ \forall \mathbf{x} \in \partial\Omega \tag{9}$$

$$\mathbf{u}(\mathbf{x}+\mathbf{L}) = \mathbf{u}(\mathbf{L}) + \langle\epsilon\rangle \cdot \mathbf{x}\,;\ \mathbf{t}(\mathbf{x}+\mathbf{L}) = -\mathbf{t}(\mathbf{x})\,,\ \forall \mathbf{x} \in \partial\Omega \tag{10}$$

Hazanov and Huet (1994) showed that SUBC and KUBC provide – for a single VE – the lower and upper bounds of any apparent stiffness tensor obtained with MUBC as presented in equation (11).

$$\mathbf{K}_{SUBC}^{app} \leq \mathbf{K}_{MUBC}^{app} \leq \mathbf{K}_{KUBC}^{app} \tag{11}$$

In our case, the choice of the boundary conditions is restricted by the geometry of the VEs which are non periodic and present porosity connected to the boundary. The PBC cannot be used because it requires a consistent mesh at opposite sides of the VE. The same holds for SUBC because stress cannot be applied on pores connected to the boundary. Displacement controlled boundary conditions are then required.

Hazanov and Amieur (1995) introduced the "orthogonal mixed uniform boundary conditions" – a specific set of boundary conditions included into the MUBC – where the traction vector is imposed in one (or two) macroscopic direction(s) and the displacement is imposed in two (or one) orthogonal direction(s). However it requires limitations on the volume and the loading to satisfy the Hill condition. Indeed the microstructure within the VE must be at least orthotropic and shear loadings cannot be applied, so the apparent stiffness tensor cannot be fully determined (see Hazanov (1998)). To deal with these restrictions – mainly the second one – Pahr and Zysset (2008) define a special set of mixed boundary conditions called "periodic compatible mixed boundary conditions" for six independent strain load cases. These boundary conditions return the same overall elastic properties than PBC for an orthotropic microstructure. But the Hill condition is not fully satisfied in the case of SiC/SiC VE, and the computation of the apparent stiffness tensor using the mechanical method defined in equation (2) leads to a slightly non symmetric tensor. So it is necessary to use the energetic definition (equation (3)) which ensures the perfect symmetry of $\mathbf{K}^{app}$.

To summarise, the apparent behaviour is determined by the finite elements method (using prismatic elements in Cast3m, http://www-cast3m.cea.fr) by the energetic approach using KUBC and the set of mixed boundary conditions proposed by Pahr and Zysset (2008) (called in the next sections MBC). Note that PBC were applied on the two faces of the VE which are perpendicular to the fibres direction.

3 Fluctuations and homogeneous equivalent behaviour

3.1 Apparent behaviour fluctuations

In order to deal with the RVE question, numerical simulations are conducted on a large number of VEs. As presented on Figure 5, four VE sizes were studied (see Table 2).

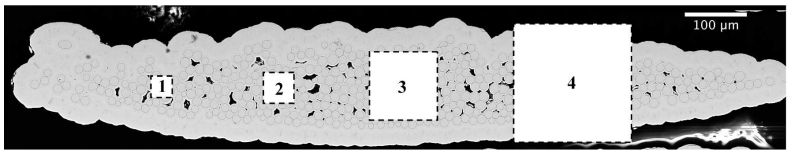

Figure 5: Sizes of the VEs compared to the size of a tow

	Size 1	**Size 2**	**Size 3**	**Size 4**
L (µm)	35.6	40.5	110.5	192
δ	5.5	6.2	17	29.5
N	5	10	50	150

Table 2: VEs data (where L is the side length, δ is the side length over the average fibres' radius and N is the average number of fibres)

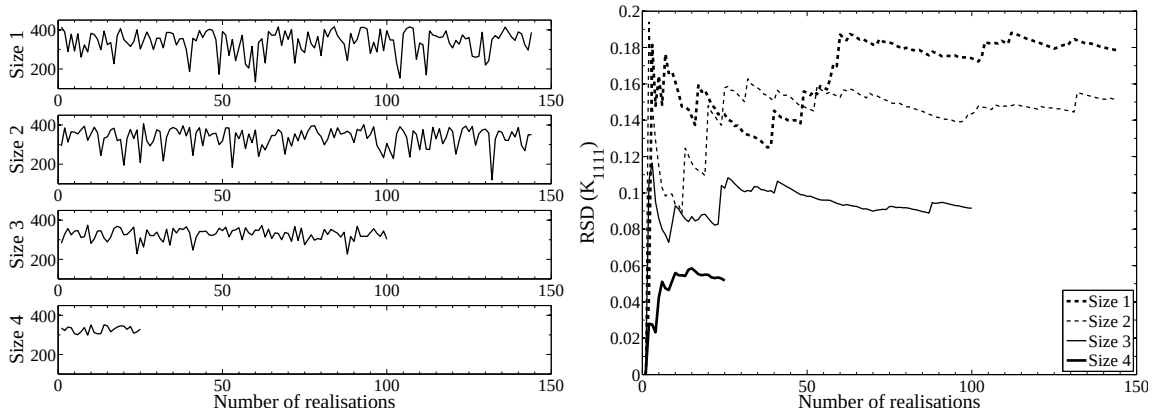

(a) Evolution of K_{1111} (GPa) versus the different statistic realisations for the four VE sizes

(b) Relative standard deviation of K_{1111} for the four VE sizes

Figure 6: Characterisation of the fluctuations of the apparent behaviour (K_{1111}, MBC)

First, the fluctuations of $\mathbf{K}^{app}$ are studied for both types of boundary conditions and the four sizes of VE, and Figure 6 illustrates the results presenting the fluctuations of the first coefficient of the tensor (using notation in an orthonormal basis, where the direction 1 is parallel to one side of the VE). Figure 6a shows that variations are very strong for the first three sizes and the smaller the VEs, the stronger the variations. Indeed the Relative Standard Deviation (RSD) – defined as the standard deviation over the average – decreases from 18% for size 1 to 5% for size 4 (see Figure 6b). The fluctuations are too pronounced for the 2 smallest sizes, whereas they are the only VEs which reasonnably satisfy the separability of scales criterion (see Section 2.2). That means that the size of the RVE is too large compared to the size of the tow and a homogeneous equivalent behaviour cannot be strictly defined for the tow.

3.2 Estimate of the homogeneous equivalent behaviour

It is still an open issue how to take into account these fluctuations in structural computations. As a first approximation these variations are neglected and the homogeneous equivalent behaviour is proposed to be evaluated by averaging the apparent behaviours of several VEs smaller than the RVE. Such volumes are called Statistical Volume

Elements (SVE). A SVE takes heed of a part of the heterogeneity and the random nature of the microstructure (see Ostoja-Starzewski (2006); Yin et al. (2008)). The use of VEs smaller than the RVE has to be offset by averaging the apparent behaviour of several SVEs. As shown by Huet (1990) in equation (12) the homogeneous equivalent behaviour is bounded by the average over a large number of configurations of SVEs' apparent behaviours resulting of SUBC and KUBC. In this paper one can only use the upper bound and an estimate provided by the average over all configurations computed with MBC. Finally, note that the average value given by any boundary conditions could lead to a different estimate than the one obtained from the RVE if the SVEs are too small (Kanit et al. (2003); Ostoja-Starzewski (1998)).

$$\langle \mathbf{S}^{app}_{SUBC} \rangle^{-1} \leq \mathbf{K}^{eff} \leq \langle \mathbf{K}^{app}_{KUBC} \rangle \tag{12}$$

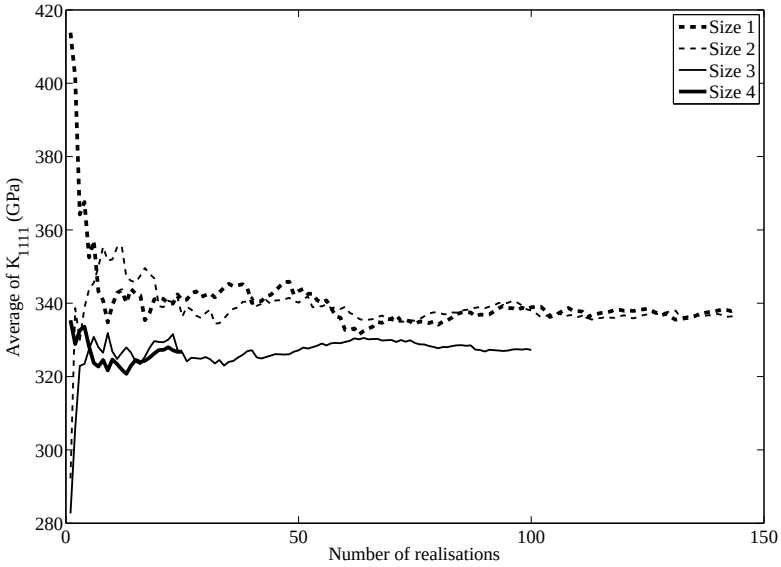

Figure 7: Average of K_{1111} over the considered number of SVE

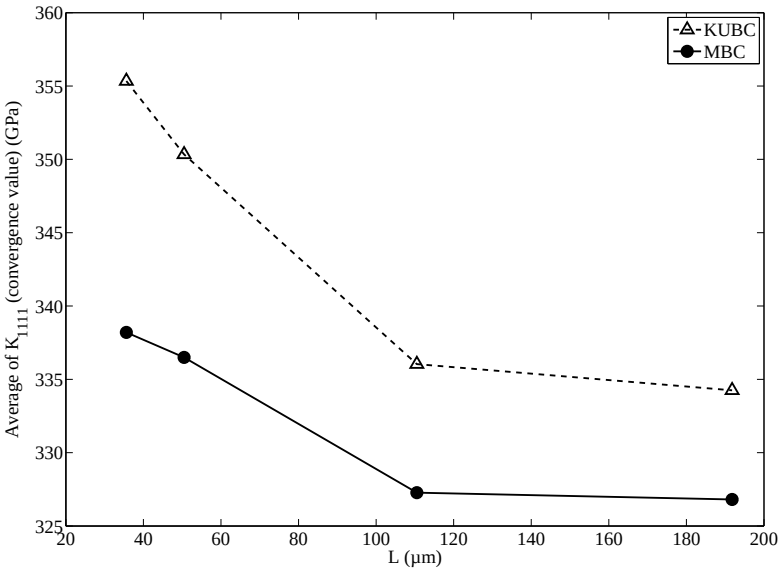

Figure 8: Average of K_{1111} versus the SVE size, for the two types of boundary conditions

Figure 7 shows the evolution of the average value over the number of considered SVEs (results from MBC) for the four SVE sizes. It confirms that the average converges to different values depending on the size of the SVE. Furthermore the number of SVE simulations necessary for the average to converge decreases when the SVE size increases: 81, 52 , 36 and 5 SVEs are necessary for the mean coefficients to be located within a $\pm$ 2% error for size 1, 2, 3 and 4, respectively. Both size and boundary conditions effects on the average of K_{1111} (computed on

all SVEs) are presented in Figure 8. The average depends indeed on the SVE size, and it stabilizes from the size 3. Same observations can be done about the discrepancy between the two types of boundary conditions which is decreasing until 3% for size 4. The same study for all coefficients – relative to the transverse isotropy – leads to similar conclusions with effects due to the SVE size and boundary conditions more or less pronounced depending on the coefficient. Finally, the average of the apparent stiffness tensors of 5 SVEs of size 4 leads to an estimate of the homogeneous equivalent behaviour which can be considered as satisfactory because of its small dependence – less than 3% – on the boundary conditions and the size of the SVE. The average could also be computed using size 3 but it would require more simulated SVEs.

4 Effects of porosity

4.1 Pores' morphology effect

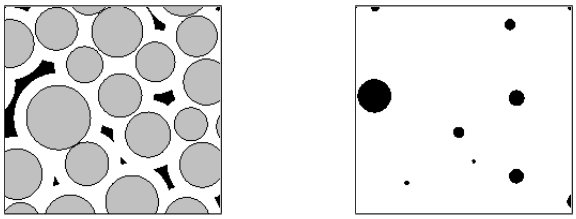

(a) CVI microscructure

(b) Microstructure with circular pores

Figure 9: Example of correspondance between CVI and circular pores microstructures

The complex and anisotropic behaviour is mainly due to the presence of voids – the pores – in the microstructure. Considering this point, the influence of the specific morphology of pores on the mechanical behaviour is studied: a microstructure with circular pores which present exactly the same barycenter and the same area than pores in corresponding CVI microstructure is built (see Figure 9). Fibres and matrix are modelled with a unique elastic isotropic matrix for which the Young's modulus is defined from the mixture law (volume averaging, E=384 GPa). Nine SVEs (size 4) of each microstructure are simulated. Table 3 compares the results concerning the characterisation of separability of scales issues – fluctuations (RSD), difference between boundary conditions – and the estimate of the homogeneous equivalent behaviour. These results show that the morphology of "real" pores is responsible for a high softening effect: the average of K_{1111} is 50 GPa less that considering circular pores (380 to 330 GPa). The real pores' morphology also makes separability of scales issues worth: though they are low, the variations of apparent behaviour and difference between KUBC and MBC are stronger. That means that microstructure with circular pores would certainly require fewer and smaller SVEs to compute a good estimate of the homogeneous equivalent behaviour. So realistic representation of the SiC/SiC microstructure cannot be avoided.

		Average K_{1111}	**RSD**	**Difference between BC**
		GPa	%	%
Circular pores	MBC	379.9	1	0.2
	KUBC	*380.7*	*1*	
Real pores	MBC	327.1	2.7	1.3
	KUBC	*331.3*	*2.1*	

Table 3: Comparison between microstructures with circular pores and "real" pores (results computed on 9 SVEs of each microstructure)

4.2 Volume fraction of porosity effect

The residual porosity is due to the deposit of matrix by CVI process, so the porosity volume fraction – through the matrix thickness – is representative for the process quality. In order to evaluate the effects of the quality of the CVI process, groups of nine SVEs (size 4) are simulated, considering that the difference between each group is the matrix thickness. Resulting volume fractions of porosity of the five tested matrix thicknesses are presented in Figure 10. The main effect is the high softening from 4% to 7% porosity (around 320 to 250 GPa, see Figure 11a) which is an interval of realistic porosity. Consequently it will be necessary to pay attention to this softening impact on the composite behaviour, when the scale transition from the tow to the woven composite is studied. The effects on fluctuations are also characterized in Figure 11b using the RSD of apparent K_{1111}. It shows that the variations are stronger for high volume fractions of porosity. Moreover, the difference between the estimated homogeneous equivalent behaviour from the two types of boundary conditions increases also with the volume fraction of porosity (see Figure 11a). So separability of scales issues are emphasized when the volume fraction of porosity increases. Then size and number of SVEs necessary to estimate the homogeneous equivalent may increase for high volume fractions of porosity.

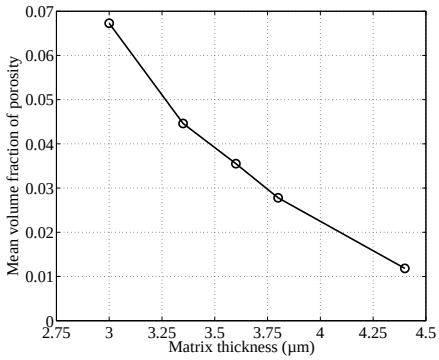

Figure 10: Evolution volume fraction of porosity over simulated matrix thicknesses

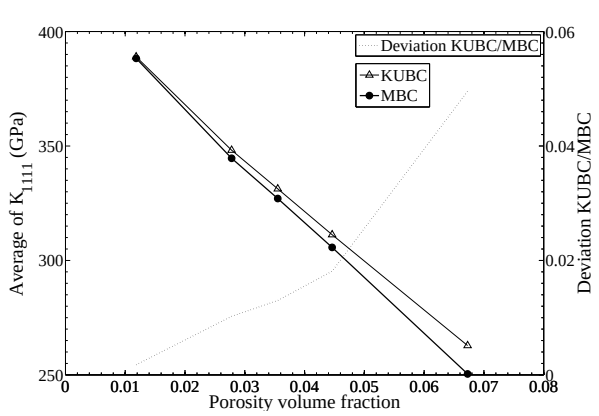

(a) Average value of K_{1111} and difference between the two types of boundary conditions over the volume fraction of porosity

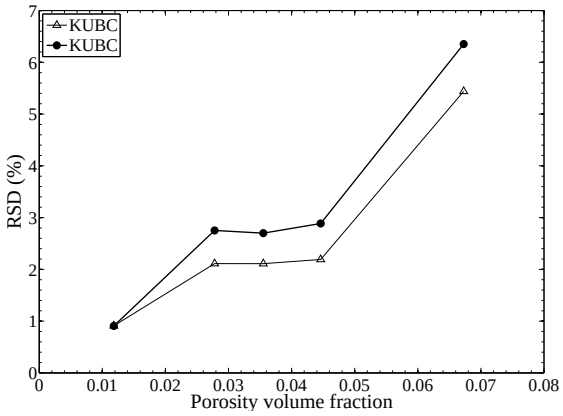

(b) Relative standard deviation of apparent K_{1111} versus the volume fraction of porosity

Figure 11: Effects of volume fraction of porosity on fluctuations of apparent K_{1111} and on the average of K_{1111}

5 Conclusion

A significant characterisation of the microstructure has been presented, based on FEG-SEM images analysis of several tows within a section of a woven composite. These characteristics are the foundation of the random generation of a virtual microstructure representative of the real material. The used algorithm does not allow to generate high volume fraction of fibres (55% instead of 58%), but the mean volume fraction of porosity is correct thanks to the matrix thickness adjustment. Another algorithm based on rearrangement procedure is under development to generate microstructures with higher surface fractions of fibres. A numerical procedure has been used to simulate a high number of Volume Elements (VEs) to deal with the Representative Volume Element (RVE) question.
The elastic problem of homogenisation has been solved with mechanical calculations using a finite element code. Kinematic Uniform and Mixed Boundary Conditions have been applied on these porous random microstructures to compute the apparent stiffness tensor. The numerical results concerning four sizes of VEs lead to the following conclusions:

1. The apparent behaviour is too sensitive to the statistic realisation if considered VEs are too small, but the variations can be neglected only for too large VEs. The RVE is too large compared to the size of the tow. This microstructure does not satisfy the separability of scales criterion, as a consequence a homogeneous equivalent behaviour cannot be strictly defined for the tow.

2. In a first approximation, fluctuations are neglected and the homogeneous equivalent behaviour is proposed to be evaluated by averaging the apparent behaviour of several Statistical Volume Elements (SVEs) – smaller than the RVE. It has been shown that an average using 5 SVEs containing about 150 fibres leads to a satisfying estimate of the homogeneous equivalent behaviour thanks to its small dependence to the boundary conditions and to the size of the SVEs.

3. The specific morphology of porosity is responsible for softening the mechanical properties, compared to the equivalent microstructure containing circular pores. This softening is getting worse with variations of volume fraction of porosity – representative of the quality of the matrix infiltration process – and it is not negligible at the scale of the tow. Finally, separability of scales issues are not only due to the heterogeneous voids distribution but also to the specific morphology of the pores and an increase of volume fraction of porosity also makes fluctuations of the apparent behaviour and difference between boundary conditions more important.

These conclusions need to be reinforced by stress and strain heterogeneities studies before the transfer to the scale of the woven composite, where the consideration of the fluctuations and the effects of volume fraction of porosity will be tackled.

References

Bornert, M.; Bretheau, T.; Gilormini, P.: *Homogénéisation en mécanique des matériaux*, vol. 1. Hermès Science Publications (2001).

Gélébart, L.; Chateau, C.; Bornert, M.; Crépin, J.; Boller, E.: X-ray tomographic characterization of the macroscopic porosity of CVI SiC/SiC composites, effects on the elastic behaviour. *Int. J. Appl. Ceram. Tec.*, accepted octobre 2009.

Gélébart, L.; Colin, C.: Effects of porosity on the elastic behaviour of CVI SiC/SiC composites. *J. Nucl. Mater.*, 386, (2009), 82–85.

Hazanov, S.: Hill condition and overall properties of composites. *Arch. Appl. Mech.*, 68, 6, (1998), 385–394.

Hazanov, S.; Amieur, M.: On overall properties of elastic heterogeneous bodies smaller than the representative volume. *Int. J. Eng. Sci.*, 33, 9, (1995), 1289–1301.

Hazanov, S.; Huet, C.: Order relationships for boundary-conditions effect in heterogeneous bodies smaller than the representative volume. *J. Mech. Phys. Solids*, 42, 12, (1994), 1995–2011.

Huet, C.: Application of variational concepts to size effects in elastic heterogeneous bodies. *J. Mech. Phys. Solids*, 38, 6, (1990), 813–841.

Jiang, M.; Jasiuk, I.; Ostoja-Starzewski, M.: Apparent elastic and elastoplastic behavior of periodic composites. *Int. J. Solids Struct.*, 39, 1, (2002), 199–212.

Kanit, T.; Forest, S.; Galliet, I.; Mounoury, V.; Jeulin, D.: Determination of the size of the representative volume element for random composites: statistical and numerical approach. *Int. J. Solids Struct.*, 40, 13-14, (2003), 3647–3679.

Ostoja-Starzewski, M.: Random field models of heterogeneous materials. *Int. J. Solids Struct.*, 35, 19, (1998), 2429–2455.

Ostoja-Starzewski, M.: Material spatial randomness: From statistical to representative volume element. *Probabilist. Eng. Mech.*, 21, 2, (2006), 112–132.

Pahr, D. H.; Zysset, P. K.: Influence of boundary conditions on computed apparent elastic properties of cancellous bone. *Biomech. Model. Mechan.*, 7, 6, (2008), 463–476.

Yin, X. L.; Chen, W.; To, A.; McVeigh, C.; Liu, W. K.: Statistical volume element method for predicting micro structure-constitutive property relations. *Comput. Method. Appl. M.*, 197, 43-44, (2008), 3516–3529.

Addresses: Camille Chateau and Lionel Gélébart, CEA Saclay, DEN/DANS/DMN/SRMA, 91191 Gif/Yvette Cedex, France.
Michel Bornert, Unité de Recherche Navier, Ecole des Ponts ParisTech, Université Paris Est, 77455 Marne-la-Vallée Cedex, France
Jérôme Crépin, Centre des matériaux, Mines ParisTech, CNRS UMR 7633, BP 87, 91003 Evry Cedex, France.
Camille Chateau and Daniel Caldemaison, Laboratoire de Mécanique des Solides, Ecole polytechnique, CNRS UMR 7649, 91128 Palaiseau Cedex, France.
email: `camille.chateau@cea.fr .`